Journal of Electroanalytical Chemistry 815 (2018) 114–122

Contents lists available at ScienceDirect

Journal of Electroanalytical Chemistry

journal homepage: www.elsevier.com/locate/jelechem

Cationic diodes by hot-pressing of Fumasep FKS-30 ionomer film onto a microhole in polyethylene terephthalate (PET)

Luthando Tshwenya[a,b,c], Omotayo Arotiba[a,c,d], Budi Riza Putra[b,e], Elena Madrid[b], Klaus Mathwig[f], Frank Marken[b,*]

[a] Department of Applied Chemistry, University of Johannesburg, Doornfontein 2028, South Africa
[b] Department of Chemistry, University of Bath, Bath BA2 7AY, UK
[c] DST/Mintek Nanotechnology Innovation Centre, University of Johannesburg, South Africa
[d] Centre for Nanomaterials Science Research, University of Johannesburg, South Africa
[e] Department of Chemistry, Faculty of Mathematics and Natural Sciences, Bogor Agricultural University, Bogor, West Java, Indonesia
[f] University of Groningen, Groningen Research Institute of Pharmacy, Pharmaceutical Analysis, P.O. Box 196, 9700 AD Groningen, The Netherlands

ARTICLE INFO

Keywords:
Membrane
Transistor
Ion pump
Desalination
Energy harvesting

ABSTRACT

A cationic diode is fabricated by hot-pressing a commercial cation-conducting ionomer membrane (Fumasep FKS-30) onto a polyethylene terephthalate (PET) substrate with microhole of 5, 10, 20, or 40 μm diameter. Both, symmetric (ionomer on both sides) and asymmetric (ionomer only on the working electrode side) cases are investigated in a 4-electrode measurement cell. A 5-electrode measurement cell in generator-collector mode is employed to directly detect competing proton transport through the ionomer. Only the asymmetric device allows ion current rectification to be observed. With decreasing microhole diameter the rectification effect increases. With increasing electrolyte concentration (for aqueous HCl, NaCl, LiCl, NH_4Cl, $MgCl_2$, $CaCl_2$) the rectification effect diminishes. Competition between cation transport and proton transport is observed in all cases. A qualitative impedance model is developed to diagnose the quality and performance of these cationic diodes.

1. Introduction

Ionomer films are routinely applied in membrane materials, which are crucially important in many areas of electrochemistry including fuel cells [1], electrosynthesis [2], and in desalination devices [3]. Semi-permeable ionomer films (such as those based on Nafion [4–6]) are widely used and have recently been shown to also allow ionic current rectifiers to be designed [7]. The function of these ionic current rectifiers has been modelled [8] and suggested to be linked to both local concentration/conductivity changes and polarisation at the ionomer | electrolyte interfaces. These ionic current rectifiers or ionic diodes could have potential for application in “iontronics” [9] or in ionic energy conversion [10,11]. Recently, a wider range of ionomer film materials attached to a poly-ethylene-terephthalate (PET) substrate with a microhole have been shown to exhibit ionic rectification effects, which lead to “ionic diode” behaviour. For cation-conducting cellulose films [12] “cationic diode” phenomena were demonstrated, and for polymer of intrinsic microporosity (PIM) films pH-switchable diode phenomena were reported [13,14]. These ion current rectification effects could be of interest in polymer or cellulose-based water purification and desalination [15], but possibly also in energy conversion [16] and in sensing [17]. Therefore, it is interesting to explore ion transport and rectification phenomena as a function of ionomer material and of diode geometry. In contrast to studies with drop-cast ionomer materials, more defined ionic diode geometries are possible, for example, by hot-pressing ionomer film of defined thickness onto a PET support film with microhole.

Ionic diode or ion current rectification effects are associated with the ability of ion channels to undergo structural changes under applied voltage bias. Many examples are known for nano-channel diodes [18,19] in which double layer and compositional changes create localised depletion/accumulation effects leading to “closed” and “open” diode behaviour. Bockris reported electrolytic diodes [20], which rely on the formation of ion depletion and ion accumulation zones. Today, a wider range of electrolytic rectifiers is known [21] and novel diodes based, for example, on asymmetric permselective membranes [22] and on chemical precipitation reactions [23] have been reported. If properly understood, developed, and optimised, the ability of ionic diodes to allow or inhibit ions to pass through could be used as a separation technique to treat wastewater and to selectively remove some toxic

* Corresponding author.
E-mail address: f.marken@bath.ac.uk (F. Marken).

https://doi.org/10.1016/j.jelechem.2018.03.027
Received 27 November 2017; Received in revised form 11 March 2018; Accepted 12 March 2018
Available online 12 March 2018
1572-6657/

heavy metals and/or anions from waste streams.

This study aims to introduce hot-pressing as a technique for fabricating ionic diodes with defined geometric dimensions from commercial Fumasep FKS-30 ionomer films and poly-ethylene-terephthalate (PET) substrates. The hot-pressing method offers a better defined ionic diode geometry, when compared to the conventional solution drop-casting and drop-drying of ionomer films on PET [24]. Fumasep FKS-30 ionomer membranes are employed here as cation conducting membranes [25]. Reported properties of Fumasep FKS-30 ionomer films are high permselectivity and an ion exchange capacity (IEC) of 1.3 to 1.4 meq/g dry membrane [26]. This corresponds to an equivalent weight of 1 / IEC = 740 Da close to that reported for Nafion ionomer materials. The water transference associated with cation transport in Fumasep FKS-30 has been investigated [27]. There is also a recent report on the application of Fumasep membranes in desalination technology [28]. It is shown here that hot-pressing allows cationic diodes to be fabricated and that the resulting rectification phenomena are dependent on microhole diameter, electrolyte concentration, and the nature of the electrolyte. Significant competition of cation transport with proton transport is observed.

2. Experimental

2.1. Materials

Poly-ethylene-terephthalate (PET) films of 6 µm thickness with laser-drilled micropores (of nominally 5, 10, 20 and 40 µm diameter) were obtained from Laser-Micro-Machining Ltd., Birmingham UK, and used as substrates for fabricating cationic diodes with Fumasep FKS-30 (nominally 30 µm thickness, Fuelcellstore.com) as the ionomer film. All the reagents used for preparing the solutions were analytical or reagent grade and were purchased from Sigma-Aldrich (UK).

2.2. Instrumentation

The ionic diodes were fabricated using a Swing Away heat-press machine (HP230B, Amazon, UK). All electrochemical measurements were recorded either using an Autolab potentiostat (GPSTAT, Eco Chemie, NL) or using a Solartron 1286/1250 potentiostat/analyser combination in a conventional four-electrode configuration (see Fig. 1) and by employing a measurement cell based on two electrolyte-filled half-cells separated by the membrane [13]. One half-cell contains the Pt wire working electrode and a saturated calomel (SCE) sense electrode and the other half-cell contains the SCE reference and Pt wire counter electrodes. In some experiments a second working electrode is introduced (in the five-electrode configuration, see below) to monitor proton transport through the diode.

2.3. Procedures for membrane fabrication

To form an asymmetric diode, a 1 cm^2 piece of Fumasep FKS-30 film was cut out and placed on top of a PET film (covering the microhole). The assembly was sandwiched between two Teflon films followed by hot pressing on a preheated hot-press (180 °C) for 45 min. To form a symmetric diode a procedure like the one used above, however, two 1 cm^2 Fumasep FKS-30 pieces are placed opposite to each other with the PET film sandwiched, followed by hot-pressing between two Teflon films for 45 min. Ionic diodes obtained in this way are reasonably robust, but weak adhesion between ionomer and PET does cause occasional delamination, particularly at higher applied potentials. Therefore, applied potentials in this study are limited to ± 2 V.

Fluorescence imaging experiments were performed on a Carl Zeiss Confocal Scanning Microscope. A Fumasep FKS-30 film was soaked for 5 h in a dilute rhodamine B solution (*ca.* 0.1 mM in water), after which the film was rinsed thoroughly and dried at 50 °C in an oven. The (partially) dyed film was then hot-pressed on PET as previously described, and placed on a glass substrate for fluorescence imaging (Fig. 1).

3. Results and discussion

3.1. Assembly of symmetric and asymmetric membrane architectures

Hot-pressing was selected as a convenient process for producing ionic diodes based on approximately 1 cm^2 pieces of Fumasep FKS-30 (nominally 30 µm thickness) and a 5 cm × 5 cm PET substrate (6 µm thickness) with central microhole (typically 20 µm diameter). The temperature was increased to improve adhesion and after optimisation 45 min of 180 °C was selected for “asymmetric” films. For “symmetric” membranes the Fumasep FKS-30 ionomer was placed both below and above the PET substrate. Fig. 1A shows a multi-stack fluorescence microscopy image as top view (with focus on the PET layer) and as side view. The rhodamine B dye (only used here for fluorescence microscopy) can be seen to have penetrated only partially (*ca.* 5 µm deep) into the Fumasep FKS-30 films therefore giving fluorescent layers at the location of the ionomer surfaces. Fig. 1A shows the symmetric membrane assembly with the PET substrate in the middle. The top view shows the approximately 20 µm diameter microhole, but also some PET

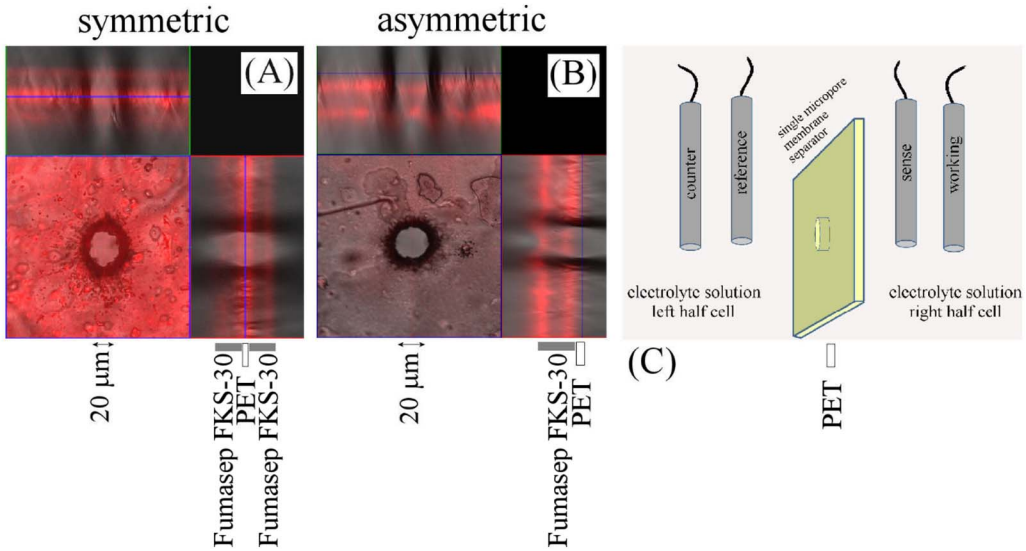

Fig. 1. Confocal microscopy image (fluorescence from rhodamine B dye partially adsorbed into the surface of the Fumasep FKS-30 film) for (A) a symmetric device with Fumasep FKS-30 on both sides of the PET film and (B) an asymmetric device with Fumasep FKS-30 only on one side. (C) Schematic drawing of the 4-electrode configuration for membrane voltammetry and impedance with ionomer films always on the side of the working electrode.

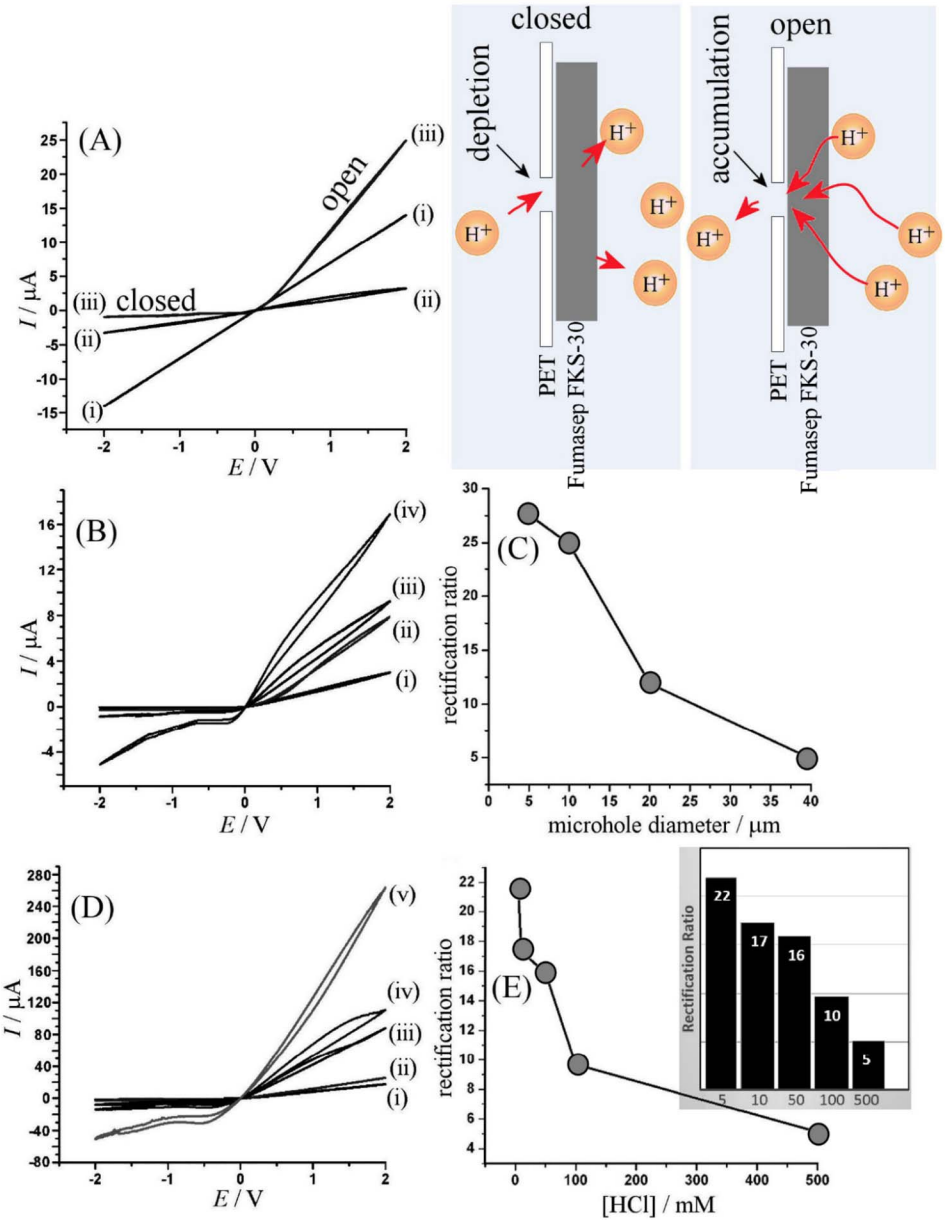

Fig. 2. (A) Cyclic voltammograms (scan rate 50 mV s^{-1}) in 10 mM HCl for (i) an empty 20 µm diameter PET microhole, (ii) a symmetric device, and (iii) the asymmetric device. For the asymmetric case "open" and "closed" diode states are indicated and explained with a schematic drawing. (B) Cyclic voltammograms (scan rate 50 mV s^{-1}, asymmetric) in 10 mM HCl for a microhole of (i) 5, (ii) 10, (iii) 20, and (iv) 40 µm diameter. (C) Plot of rectification ratio (= absolute current ratio at +1/−1 V) *versus* microhole diameter. (D) Cyclic voltammograms (scan rate 50 mV s^{-1}, 20 µm diameter microhole, asymmetric) in (i) 5, (ii) 10, (iii) 50, (iv) 100, and (v) 500 mM HCl. (E) Plot of rectification ratio *versus* HCl concentration (inset: bar plot).

debris from the laser drilling process. The side view reveals some optical fringe effects in particular in the microhole region. Fig. 1B shows the asymmetric membrane with a similar pattern of fluorescence intensity at the Fumasep FKS-30 ionomer film surface.

3.2. Electrochemical characterisation I.: effects of geometry and concentration in aqueous HCl

When performing voltammetry experiments, aqueous electrolyte (10 mM HCl) was employed on both sides of the 4-electrode measurement cell (Fig. 2C). For the case of an un-modified PET microhole of 20 µm diameter (Fig. 2Ai) a straight line voltammogram consistent with resistance (here R = 0.13 MΩ) is observed. Based on the equation for microhole resistance (Eq. (1) [29]) this value can be explained based on three components (assuming an approximate microhole radius of $r = 10$ µm and PET film thickness $L = 6$ µm) with a specific conductivity of $\kappa = 0.53\ \Omega^{-1}\ m^{-1}$ for 10 mM HCl, which is in reasonable agreement with literature values [30,31].

$$resistance = \frac{1}{4\kappa r} + \frac{L}{\pi\kappa r^2} + \frac{1}{4\kappa r} \quad (1)$$

In this equation the overall resistance is given by a first term for the access resistance (for the counter electrode side), a second term for the solution contained within the cylindrical microhole, and a third term for access resistance (for the working electrode side) [32]. This equation assumes that for a small enough microhole diameter the bulk electrolyte resistance can be neglected (*vide infra*).

When applying the Fumasep FKS-30 ionomer film to both sides of the PET microhole ("symmetric", Fig. 2Aii) the overall resistance can be seen to be increased in spite of Fumasep FKS-30 ionomer being similarly ionically conductive compared to aqueous 10 mM HCl. This observation is likely to be linked to the internal trapped volume (between the two ionomer films) not being fully/reproducibly flooded with electrolyte solution or air-trapping. This symmetric geometry is therefore not useful for quantitative measurements. However, when investigating the "asymmetric" case, well-defined voltammetric responses are observed (see Fig. 2Aiii) and two effects are apparent: (i) the current in the negative potential range is lower compared to that for the unmodified PET and (ii) the current in the positive potential range is

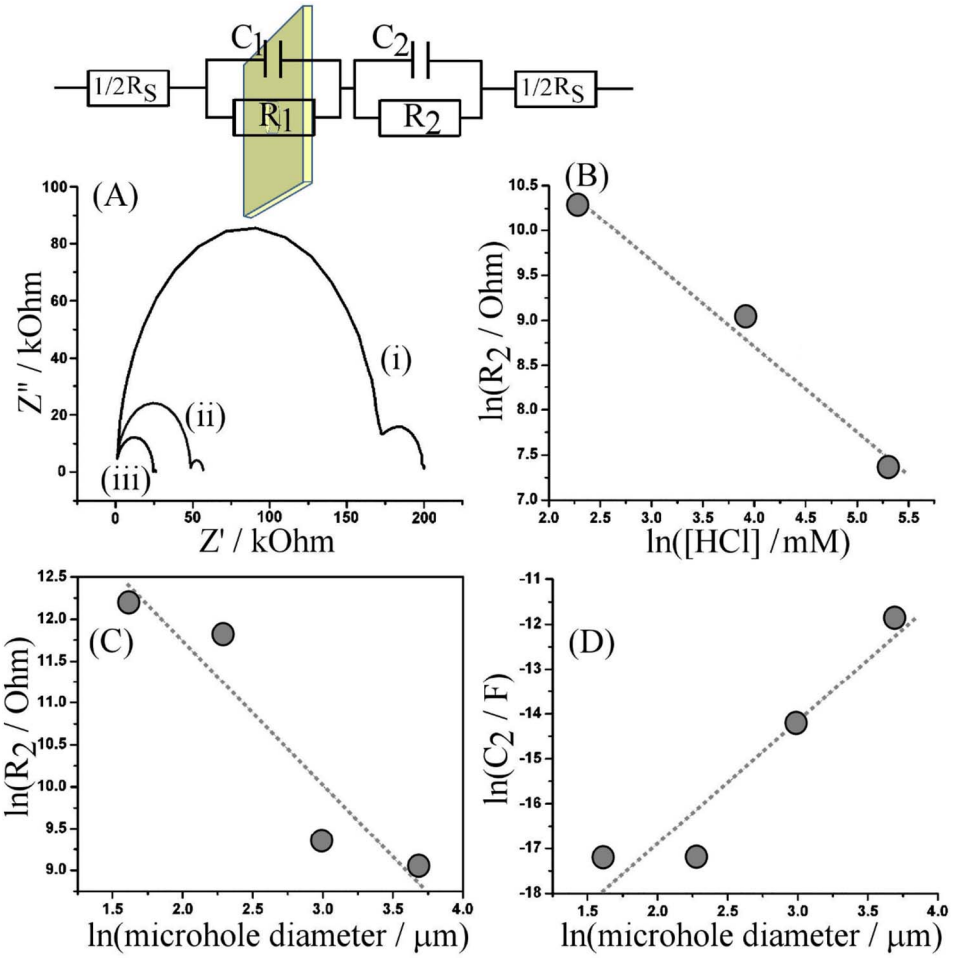

Fig. 3. (A) Impedance data (Nyquist plots measured from 60 kHz to 0.1 Hz; 10 points per decade; amplitude 100 mV; 0.0 V) for Fumasep FKS-30 ionomer attached to a 20 μm microhole PET film for (i) 10, (ii) 50, and (iii) 200 mM HCl (inset showing the circuit for fitting). (B) Double logarithmic plot of R_2 *versus* HCl concentration. (C) Double logarithmic plot of R_2 *versus* microhole diameter. (D) Double logarithmic plot of C_2 *versus* microhole diameter.

Table 1
Summary of impedance data for Fumasep FKS-30 films on PET microhole substrates under 4-electrode conditions in aqueous HCl (amplitude 100 mV; frequency range from 60 kHz to 0.1 Hz; 0.0 V; device-to-device errors estimated typically ± 30%).

Parameters/ conditions	R_S/Ω	R_1/kΩ	R_2/kΩ	C_1/nF	C_2/nF	τ_1[c]/ms	τ_2[c]/ms
10 mM[a]	1060	170	28	0.59	363	1×10^{-1}	10
50 mM[a]	445	48	8.1	0.56	2167	3×10^{-2}	17
200 mM[a]	50	24	1.6	0.52	22,900	1×10^{-2}	37
5 μm[b]	617	1220	203	0.54	36	7×10^{-1}	7
10 μm[b]	1554	840	138	0.56	32	5×10^{-1}	4
20 μm[b]	1476	233	28	0.51	670	1×10^{-1}	19
40 μm[b]	935	101	9	0.52	6932	5×10^{-2}	62

[a] Concentration of HCl when employing a 20 μm diameter microhole.
[b] Microhole diameter when employing 10 mM HCl aqueous electrolyte.
[c] $\tau_1 = R_1 \times C_1$ and $\tau_2 = R_2 \times C_2$.

increased when compared to the case of the unmodified PET. This is consistent with cationic diode behaviour [7]. A schematic drawing in Fig. 2A explains this phenomenon qualitatively based on the cation conducting behaviour in the Fumasep FKS-30 ionomer. In the "closed" state of the diode cations from the solution phase deplete (thereby decreasing local conductivity) close to the highly conducting ionomer and in the "open" state cations emerging from the highly conducting ionomer accumulate (thereby further increasing local conductivity). This type of behaviour is consistent with that observed previously for similar "cationic diodes" [7]. The slope from the open state current in the positive potential range suggests an approximate resistance of 77 kΩ associated mainly with the Fumasep FKS-30 film resistivity (*vide infra*).

When investigating the effects of the microhole diameter (Fig. 2B), it can be observed that the current increases proportionally with diameter. For a bigger microhole, the current in the open state (positive potential range) is increased due to the increased area of active Fumasep FKS-30 ionomer (see the first term for access diffusion in eq. 1) and the current in the closed state (negative potential range) is increased mainly due to the increase in the rate of diffusion-migration in the electrolyte phase. The absolute ratio of currents at +1 V and at −1 V is defined here as rectification ratio and is employed as a measure of diode performance. The plot in Fig. 2C suggests that the rectification ratio is increased for a smaller PET microhole diameter (*i.e.* with decreasing microhole diameter, the current decreases more rapidly in the closed state compared to that in the open state).

The effect of HCl electrolyte concentration on the currents for the cationic diode is shown in Fig. 2D (for a 20 μm diameter microhole). A very similar pattern emerges with an increase in HCl concentration causing an increase in both the current in the open state (the conductivity of the Fumasep FKS-30 ionomer is increased) and the current in the closed state (access diffusion-migration to the microhole is enhanced, but also concentration polarisation effects and additional anion transport through the membrane at higher electrolyte concentration need to be considered). Note the onset of over-limiting behaviour at potentials negative of −1 V. A plot of the rectification ratio *versus* HCl concentration is shown in Fig. 2E (also as bar plot inset). Clearly, for

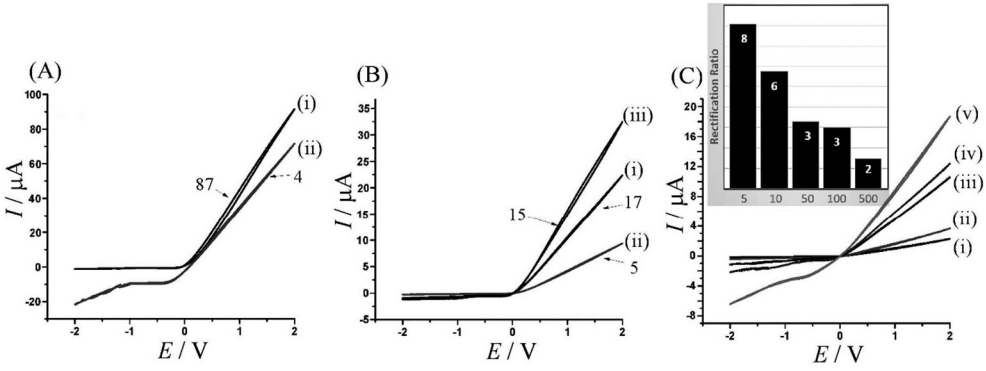

Fig. 4. (A) Cyclic voltammograms (scan rate 50 mV s^{-1}) for Fumasep FKS-30 supported on a PET substrate with a 20 µm diameter microhole and with (i) 200 mM HCl in the working electrode compartment and 10 mM HCl in the counter electrode compartment or (ii) *vice versa*. (B) Cyclic voltammograms for (i) 10 mM HCl, (ii) 10 mM NaCl, and (iii) 10 mM HCl and 10 mM NaCl. (C) Cyclic voltammograms for (i) 5, (ii) 10, (iii) 50, (iv) 100, and (v) 500 mM NaCl (inset: bar plot for rectification ratio at +1/−1 V).

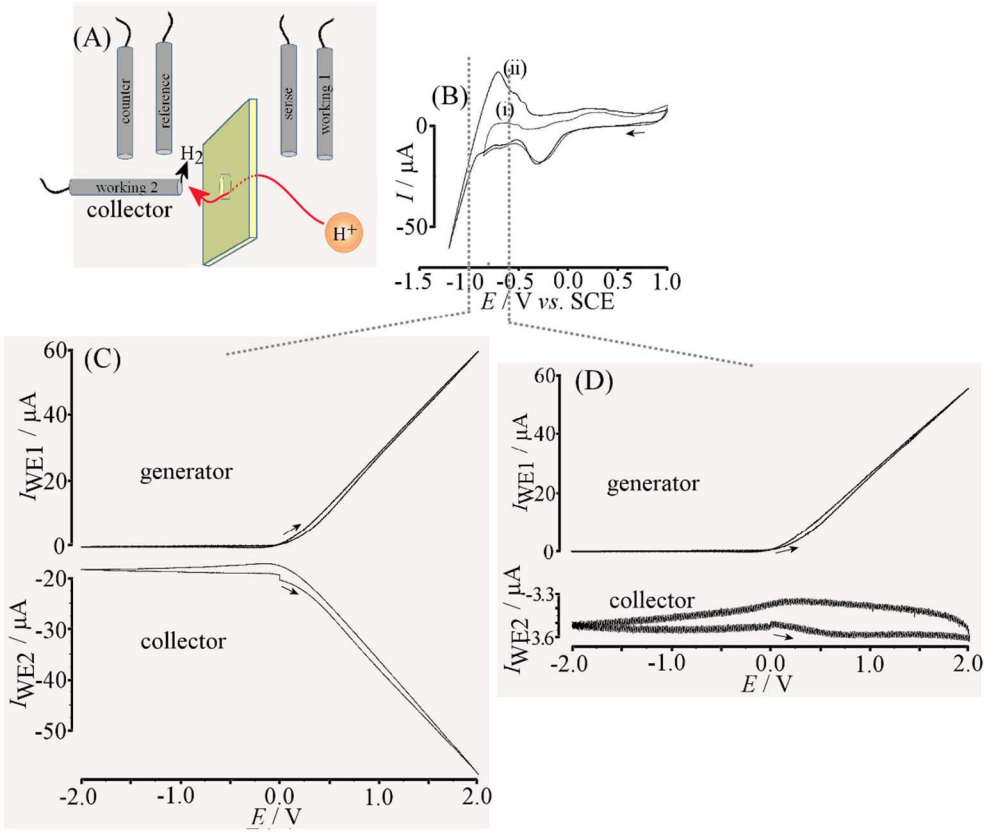

Fig. 5. (A) Schematic drawing of the 5-electrode measurement cell. (B) Cyclic voltammogram (50 mV s^{-1}) for a 3 mm diameter Pt disk electrode in 10 mM NaCl. Next, generator-collector voltammograms are shown (scan rate 50 mV s^{-1}) for E_{WE2} at fixed potential of (C) −1.0 V *vs.* SCE, and (D) −0.6 V *vs.* SCE with 10 mM HCl in the working electrode compartment and 10 mM NaCl in the counter electrode compartment and a Fumasep FKS-30 on PET with 20 µm diameter microhole.

this geometry with the Fumasep FKS-30 film hot-pressed onto the PET film with microhole, the increase in HCl concentration causes a loss in rectification ratio. There are mainly two contributions to this effect: (i) the higher electrolyte concentration may affect the semi-permeability of the Fumasep FKS-30 film thereby allowing the transport of some anions and/or (ii) the effect of electrolyte concentration on the current in the closed state is more significant compared to that on the open state.

3.3. Electrochemical characterisation II.: diagnostic impedance

Impedance methods can be employed to provide both qualitative and better quantitative insight into time-dependent phenomena. There have been recent attempts to explore for example impedance characteristics for ionic rectifiers based on glass pipette nanopore devices [33]. Complex behaviour is expected due to a combination of time and potential dependent phenomena. Therefore, here impedance is employed only at exploratory level to provide diagnostic criteria for Fumasep FKS-30 ionic diode integrity rather than at fully quantitative level, which will require further study.

In order to explore time-dependent phenomena electrochemical impedance data are obtained first for a 20 µm microhole with asymmetric Fumasep FKS-30 ionomer attached. Fig. 3 shows a typical set of data as Nyquist plots and two semi-circular features are readily identified. The high frequency impedance is associated only with external cable and solution resistance (see R_S). In the high frequency range a first semi-circle is assigned to the charging of the PET film separating the two electrolyte half-cells. Table 1 summarises the results obtained by fitting of impedance data to the circuit shown in Fig. 3. The capacitance C_1 is consistently 0.5 ± 0.1 nF, which has been shown before [7] to be associated with the charging of the inert 6 µm thick PET film sandwiched between two aqueous electrolyte solutions. The resistor R_1 appears to be linked to the high frequency resistance of the Fumasep FKS-30 ionomer film itself with some aqueous solution contributions (access and microhole resistivity in the aqueous electrolyte, see Eq. (1)) but without solution concentration polarisation contributions. In fact, the value R_1 = 170 kΩ for 10 mM HCl (see Table 1) can be used in conjunction with Eq. (1) and the specific conductivity of 10 mM HCl (*vide supra*) to give an estimate for the Fumasep FKS-30 membrane

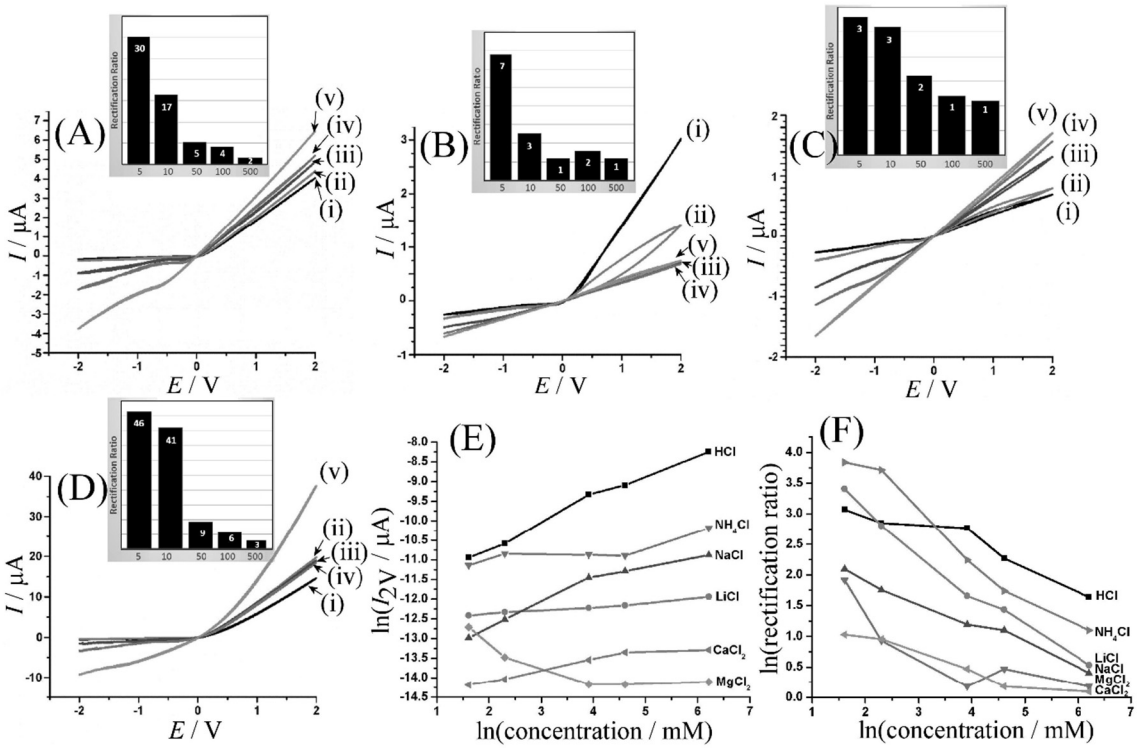

Fig. 6. (A) Cyclic voltammograms (scan rate 50 mV s^{-1}; Fumasep FKS-30) for (i) 5, (ii) 10, (iii) 50, (iv) 100, and (v) 500 mM LiCl (inset: rectification ratio). (B) As before, but for $MgCl_2$. (C) As before, but for $CaCl_2$. (D) As before, but for NH_4Cl. (E) Double logarithmic plot for currents at +2 V *versus* concentration. (F) Double logarithmic plot of rectification ratio *versus* concentration.

resistance of 87 kΩ in good agreement with the estimate obtained from cyclic voltammetry data in Fig. 2A. The specific conductivity for Fumasep FKS-30 is obtained as $1/4r\kappa_{membrane} = 87\,k\Omega$ or $\kappa_{membrane} = 0.29\,\Omega^{-1}\,m^{-1}$. In data in Fig. 3A there is a second semi-circular feature that appears at lower frequencies and which is suggested to be linked to concentration polarisation phenomena.

Data in Table 1 reveal that the resistance R_1 does have a solution component most likely associated with the liquid phase within the microhole and with the access diffusion to the microhole. Therefore effects of electrolyte concentration on R_1 are observed, but less strong compared to those for R_S. Similarly, the increase in microhole diameter causes a significant decrease in R_1 due to the larger cross-section and changes in diffusion pathway. A time constant τ_1 (typically a fraction of a ms) can be calculated associated with the charging of the PET film. Note that data for the entries for 10 mM HCl and for 20 µm microhole diameter are nominally identical and difference in the data reflects the device-to-device error margins (typically ± 20%), which is significant for R_S and C_2. Nevertheless, trends in data are useful.

The second semicircle is associated with R_2 and C_2 and a larger time constant (see τ_2 in Table 1) and believed to be linked to the ion transport processes that lead to the diode opening/closing behaviour. This time constant can be understood as the strongly diameter dependent switching time of the diode. In the double-logarithmic plot in Fig. 3B, the effect of the HCl concentration on R_2 can be seen to be associated with an exponent of approximately minus one. This is consistent with resistance being inversely proportional to electrolyte conductivity and therefore R_2 also being dominated by electrolyte resistivity. Fig. 3C shows data for R_2 as a function of microhole diameter. The approximate slope of minus two suggests a $1/r^2$ dependence as expected for the resistance of the solution volume inside of the cylindrical volume defined by the PET microhole. R_2 has to be seen as a potential dependent diode resistance, which is estimated here at an applied potential of 0.0 V. The value for R_2 is clearly lower than that observed for R_1, but more work will be needed to really resolve the physical nature of R_2. The capacitance C_2, in contrast, exhibits an r^2 dependence (see Fig. 3D) as expected for a capacitance defined by the area in the PET microhole and is suggested here to be associated with the charging of the ionomer | electrolyte interface, which is linked also to concentration polarisation.

Although not being clearly assigned to specific physical parameters, the second semi-circular feature was found to offer a good diagnostic tool for the quality of the cationic diodes produced by hot-pressing. Due to the hot-pressing process not always giving good adhesion (and possibly due to protruding PET residues from laser cutting, see Fig. 1), there are cases of this semi-circle becoming highly depressed. This can be attributed to electrolyte entering the space between PET and Fumasep FKS-30 ionomer film and causing a poor diode behaviour with a much more distributed network of ion transport pathways.

3.4. Electrochemical characterisation III.: effect of aqueous electrolytes

When investigating the rectification effects for the cationic diode based on Fumasep FKS-30 ionomer, it is interesting to also explore the case of different electrolyte concentrations in left and right half cells. Fig. 4A shows data for (i) 200 mM HCl in the working electrode compartment and 10 mM HCl in the counter electrode compartment. This is contrasted to (ii) 200 mM HCl in the counter electrode compartment and 10 mM HCl in the working electrode compartment. Clearly, a much enhanced rectification ratio of approximately 87 (compared to 3.5) is seen for a high concentration of HCl in the working electrode compartment. This observation is consistent with cations being readily "pumped" from the working electrode into the counter electrode compartment. This effect is linked to the significantly increased current in the closed state with higher electrolyte concentration in the counter electrode half-cell in contact to the PET microhole.

When comparing the behaviour of 10 mM HCl and 10 mM NaCl (Fig. 4Bi and Bii, respectively), it can be seen that HCl exhibits a higher current (presumably due to a higher diffusivity of H^+ in the Fumasep

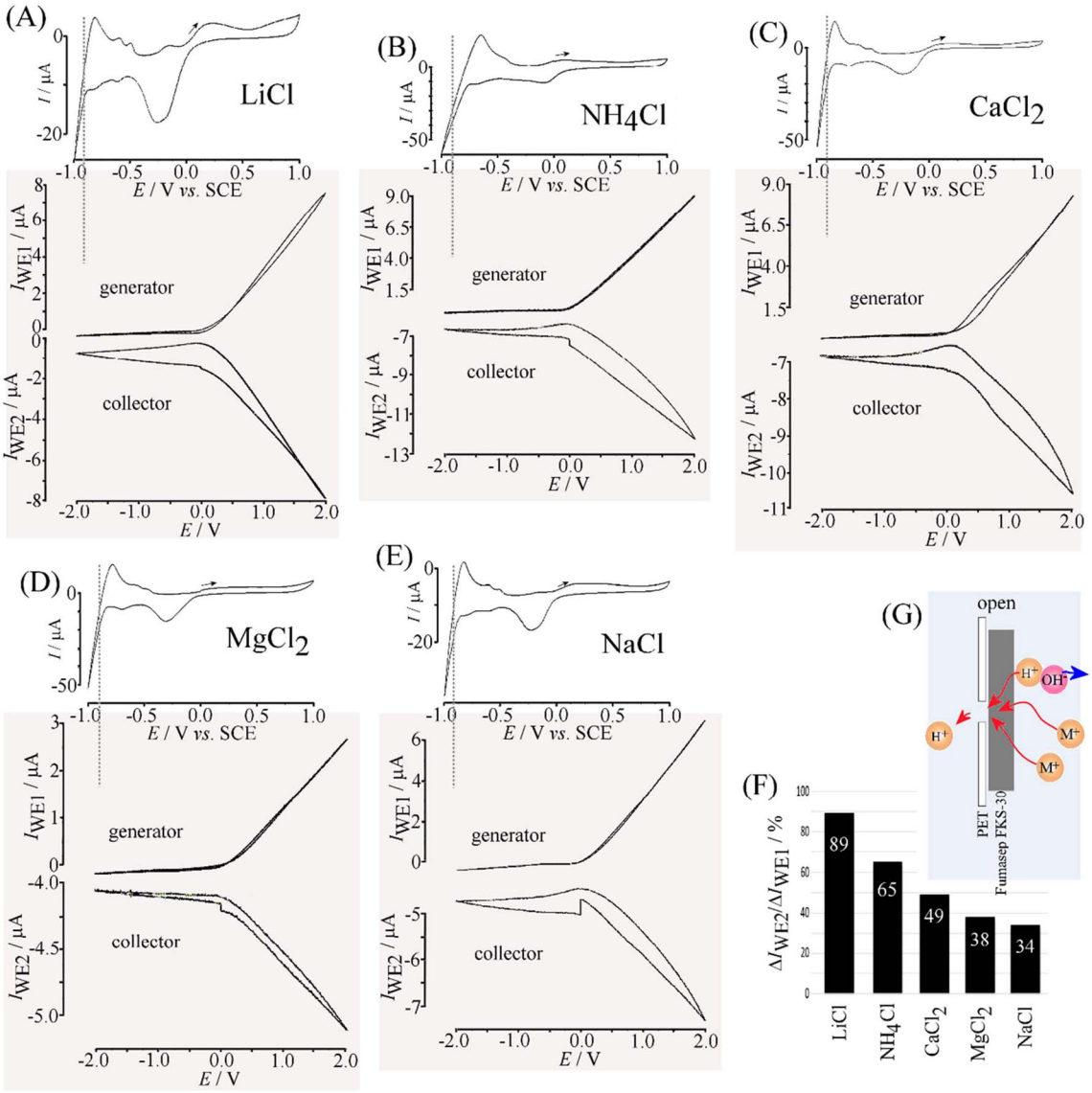

Fig. 7. (A–E) Cyclic voltammogram (3-electrode configuration; 50 mV s^{-1}) for a 3 mm diameter Pt disk electrode in (A) 10 mM LiCl, (B) 10 mM NH_4Cl, (C) 10 mM $CaCl_2$, (D) 10 mM $MgCl_2$, and (E) 10 mM NaCl. Next, generator-collector voltammograms are shown (5-electrode configuration; scan rate 50 mV s^{-1}) for E_{WE2} at fixed potential of −0.9 V *vs.* SCE and the same electrolyte in both the working electrode compartment and in the counter electrode compartment with a Fumasep FKS-30 on PET with 20 µm diameter microhole. (F) Bar plot of the working electrode 2 current divided by the working electrode 1 current (both obtained at +2 V with baseline at 0 V) to show the relative importance of trans-membrane proton transport over cation transport. (G) Schematic drawing of competing proton and cation transport.

FKS-30 ionomer) as well as a higher rectification ratio. When combining 10 mM HCl with 10 mM NaCl (see Fig. 4Biii) the current is increased, but the rectification ratio is slightly decreased. Both cations appear to contribute to the cationic diode effect. Fig. 4C shows voltammetric data for aqueous NaCl as a function of concentration (equal on both left and right side). Rectification ratios of typically 8 are reached at a low concentration of 5 mM NaCl (on both sides of the measurement cell).

It is possible to confirm the nature of the transferring cation in the charge transport process for the open state of the diode by performing a generator – collector experiment (similar to rotating ring – disk [34] or other related generator – collector experiments [35]). Fig. 5A shows a schematic drawing of the 4-electrode measurement cell with Fumasep FKS-30 cationic diode and an additional second working electrode (WE2) that is placed into the counter electrode compartment (in 10 mM NaCl) at a fixed potential. The working electrode compartment contains 10 mM HCl to allow proton transport in the open state of the diode. Both, the current through the membrane (generator; WE1) and the current at the second working electrode (collector; WE2) are monitored simultaneously. Here, a 3 mm diameter platinum disk electrode is employed to detect the proton transport by reducing protons to hydrogen. As a reference data set, Fig. 5B shows traditional cyclic voltammograms recorded for the collector electrode immersed in 10 mM NaCl. Fig. 5C and D show data for generator – collector experiments with the second working electrode either at a potential of −1.0 V *vs.* SCE or at −0.6 V *vs.* SCE, respectively. Only at −1.0 V *vs.* SCE can the proton flux be clearly identified as a conversion of protons to hydrogen (Fig. 5C). The magnitude of the collector current compared to the generator current suggests that approximately 70% of the protons crossing the membrane are detected, consistent with at least qualitative analysis of the proton flux. Data in Fig. 5D suggest only some minor current responses associated with diode opening and closing.

It is interesting to explore the effect of different types of cations on the current rectification ratio. Fig. 6 shows a summary of data for aqueous 10 mM LiCl, $MgCl_2$, $CaCl_2$, and NH_4Cl. Similar descending trends are observed for rectification ratio *versus* concentration for all,

although NH_4^+ cations appear to exhibit exceptionally high rectification effects. When plotting the current at +2 V *versus* concentration (Fig. 6E) clear differences are observed with Mg^{2+} currents even descending with higher concentration. This and the low current for Ca^{2+} are likely to be linked either (i) to lower cation mobility within the Fumasep FKS-30 ionomer or (ii) a competition of cation and proton transport.

In order to explore competition between proton and cation transport, additional experiments are performed in 5-electrode configuration (see Fig. 5A) to allow at least qualitative confirmation of proton involvement. Fig. 7 shows data obtained in generator-collector configuration for aqueous 10 mM (A) LiCl, (B) NH_4Cl, (C) $CaCl_2$, (D) $MgCl_2$, and (E) NaCl. In all cases the conventional cyclic voltammogram obtained at the 3 mm platinum disk electrode is shown with a dashed line indicating the potential for the collector. Additional experiments with the collector potential set to more positive potential confirmed a baseline response similar to that shown in Fig. 5D. From the current responses at the collector electrode it can be concluded that some proton transport is present for all cations investigated. In order to analyse the extent of proton transfer compared to cation transfer the current at +2 V is compared. The current at WE2 (platinum collector electrode) is divided by the current at WE1 (membrane current) to give a relative measure of proton involvement expressed here in % (see Fig. 7F). For Na^+ the extent of proton involvement appears to be the lowest (34%) whereas for Li^+ the value is high (89%) indicative of almost no transport of Li^+ under these conditions. Similarly, for ammonium a high level of proton transport (65%) is observed.

A schematic drawing in Fig. 7G summarises the processes of (i) M^+ cation transport *versus* (ii) H^+ proton transport associated with formation of hydroxide anions. This formation of hydroxide anions then causes localised pH changes and this explains some of the trends observed in Fig. 6E where for some cations either little increase of even a decrease in current with higher electrolyte concentration is observed. Note that further complexity may arise from possible speciation of M^{2+} cations to give mono-cations due to chloro or hydroxo ion paring and from the effects of strong hydration for the divalent cations. The implications from this work are threefold: (A) the cationic diode phenomenon may be indicative of rectified cation transport, but competition between cations and protons (from water) can interfere in the process; (B) rectification ratio data quoted for ionic diode processes can be strongly affected by this competition of cations and protons; (C) for the development of ionic diode desalination methods membrane ionomer materials with good selectivity towards the target cation/anion are needed to suppress unwanted water heterolysis.

4. Conclusions

It has been shown that cation flow rectification (or cationic diode) effects are readily achieved at asymmetric structures based on Fumasep FKS-30 ionomer film supported by a thin PET film with a microhole of typically 20 µm diameter. Voltammetry and impedance data demonstrate that diode switching occurs for 10 mM to 200 mM HCl with a time constant of 10 ms to 37 ms (for a 20 µm diameter microhole and 10 to 200 mM HCl). Many parameters affect the rectification effect (both the time constant and the rectification ratio) including electrolyte type and concentration, microhole diameter, and any differences in electrolyte solution in left and right half-cells (*e.g.* for uphill or downhill cation transport). Decreasing the diameter of the microhole may allow the rectification effect to be improved, which will be important in future applications in desalination based on arrays of cationic and anionic diodes.

Crucially, the competition of proton transport and cation transport under microhole conditions has been demonstrated to possibly severely limit any desalination capability. Qualitative estimates for proton involvement have been obtained based on 5-electrode generator-collector measurements and further work will be needed to suppress water heterolysis and proton interference. Further work will also be required to explore impedance characteristics and to improve rectification ratio values, which are here reported lower compared to those observed for drop-cast Nafion [7]. Particularly interesting will be further exploration of the cation selectivity of ionomer materials in these cationic diodes. In future, the selective removal of both higher valent cation and higher valent anions could be possible with matching cationic diodes and anionic diodes, respectively, based on the appropriate types of ionomer materials.

Acknowledgements

L.T. thanks the DST/Mintek Nanotechnology Innovation Centre, University of Johannesburg, South Africa; the Water Research Commission (grant number: K5/2567), South Africa and the National Research Foundation (CPRR grant number: 98887), South Africa for financial support. B.R.P. thanks the Indonesian Endowment (LPDP RI) for a PhD scholarship. F.M. and E.M. thank the Leverhulme Trust foundation for financial support (RPG-2014-308: “New Materials for Ionic Diodes and Ionic Photodiodes”).

References

[1] A. Kusoglu, A.Z. Weber, New insights into perfluorinated sulfonic-acid ionomers, Chem. Rev. 117 (2017) 987–1104.
[2] Y. Holade, K. Servat, S. Tingry, T.W. Napporn, H. Remita, D. Cornu, K.B. Kokoh, Advances in electrocatalysis for energy conversion and synthesis of organic molecules, ChemPhysChem 18 (2017) 2573–2605.
[3] G.M. Geise, D.R. Paul, B.D. Freeman, Fundamental water and salt transport properties of polymeric materials, Prog. Polym. Sci. 39 (2014) 1–42.
[4] J. Leddy, Modification of Nafion membranes: tailoring properties for function, in: J.L. Liu, S. Bashir (Eds.), Nanomaterials for Sustainable Energy, ACS Symposium Series 1213, Oxford University Press, Oxford, 2015, p. 99.
[5] N. Cele, S.S. Ray, Recent progress on nafion-based nanocomposite membranes for fuel cell applications, Macromol. Mater. Eng. 294 (2009) 719–738.
[6] H. Ito, T. Maeda, A. Nakano, H. Takenaka, Properties of Nafion membranes under PEM water electrolysis conditions, Int. J. Hydrog. Energy 36 (2011) 10527–10540.
[7] D.P. He, E. Madrid, B.D.B. Aaronson, L. Fan, J. Doughty, K. Mathwig, A.M. Bond, N.B. McKeown, F. Marken, A cationic diode based on asymmetric Nafion film deposits, ACS Appl. Mater. Interfaces 9 (2017) 11272–11278.
[8] K. Mathwig, B.D.B. Aaronson, F. Marken, Ionic transport in microhole fluidic diodes based on asymmetric ionomer film deposits, ChemElectroChem (2017), http://dx.doi.org/10.1002/celc.201700464.
[9] H.G. Chun, T.D. Chung, R.G. Cooks, J.E. Pemberton (Eds.), Iontronics, Ann. Rev. Anal. Chem. vol. 8, 2015, pp. 441–462.
[10] Z.J. Jia, B.G. Wang, S.Q. Song, Y.S. Fan, Blue energy: current technologies for sustainable power generation from water salinity gradient, Renew. Sust. Energ. Rev. 31 (2014) 91–100.
[11] S. Tseng, Y.M. Li, C.Y. Lin, J.P. Hsu, Salinity gradient power: influences of temperature and nanopore size, Nano 8 (2016) 2350–2357.
[12] B.D.B. Aaronson, D. Wigmore, M.A. Johns, J.L. Scott, I. Polikarpov, F. Marken, Cellulose ionics: switching ionic diode responses by surface charge in reconstituted cellulose films, Analyst 142 (2017) 3707–3714.
[13] Y.Y. Rong, Q.L. Song, K. Mathwig, E. Madrid, D.P. He, R.G. Niemann, P.J. Cameron, S.E.C. Dale, S. Bending, M. Carta, R. Malpass-Evans, N.B. McKeown, F. Marken, pH-induced reversal of ionic diode polarity in 300 nm thin membranes based on a polymer of intrinsic microporosity, Electrochem. Commun. 69 (2016) 41–45.
[14] E. Madrid, Y.Y. Rong, M. Carta, N.B. McKeown, R. Malpass-Evans, G.A. Attard, T.J. Clarke, S.H. Taylor, Y.T. Long, F. Marken, Metastable ionic diodes derived from an amine-based polymer of intrinsic microporosity, Angew. Chem. Int. Ed. 53 (2014) 10751–10754.
[15] E. Madrid, P. Cottis, Y.Y. Rong, A.T. Rogers, J.M. Stone, R. Malpass-Evans, M. Carta, N.B. McKeown, F. Marken, Water desalination concept using an ionic rectifier based on a polymer of intrinsic microporosity (PIM), J. Mater. Chem. A 3 (2015) 15849–15853.
[16] L.X. Cao, F.L. Xiao, Y.P. Feng, W.W. Zhu, W.X. Geng, J.L. Yang, X.P. Zhang, N. Li, W. Guo, L. Jiang, Anomalous channel-length dependence in nanofluidic osmotic energy conversion, Adv. Funct. Mater. 27 (2017) 1604302.
[17] B. Riza Putra, M. Carta, R. Malpass-Evans, N.B. McKeown, F. Marken, Potassium cation induced ionic diode blocking for a polymer of intrinsic microporosity (PIM) | Nafion “heterojunction” on a microhole substrate (submitted).
[18] E. Choi, C. Wang, G.T. Chang, J. Park, High current ionic diode using homogeneously charged asymmetric nanochannel network membrane, Nano Lett. 16 (2016) 2189–2197.
[19] W. Guo, Y. Tian, L. Jiang, Asymmetric ion transport through ion-channel-mimetic solid-state nanopores, Acc. Chem. Res. 46 (2013) 2834–2846.
[20] B. Loverecek, A. Despic, J.O.M. Bockris, Electrolytic junctions with rectifying properties, J. Phys. Chem. 63 (1959) 750–751.
[21] H.J. Koo, O.D. Velev, Ionic current devices-recent progress in the merging of

electronic, microfluidic, and biomimetic structures, Biomicrofluidics 7 (2013) 031501.
[22] Y. Green, Y. Edri, G. Yossifon, Asymmetry-induced electric current rectification in permselective systems, Phys. Rev. E 92 (2015) 033018.
[23] R. Zhao, G.H. He, Y.L. Deng, Non-water ionic diode based on bias-dependent precipitation, Electrochem. Commun. 23 (2012) 106–109.
[24] B.R. Putra, B.D.B. Aaronson, E. Madrid, K. Mathwig, M. Carta, R. Malpass-Evans, N.B. McKeown, F. Marken, Ionic diode characteristics at a polymer of intrinsic microporosity (PIM) | Nafion "heterojunction" deposit on a microhole poly(ethylene-terephthalate) substrate, Electroanalysis 29 (2017) 2217–2223.
[25] B.P. Zhang, J.G. Hong, S.H. Xie, S.M. Xia, Y.S. Chen, An integrative modeling and experimental study on the ionic resistance of ion-exchange membranes, J. Membr. Sci. 524 (2017) 362–369.
[26] http://www.fumatech.com/EN/Membranes/Water+treatment/Products+fumasep/.
[27] A. Zlotorowicz, R.V. Strand, O.S. Burheim, O. Wilhelmsen, S. Kjelstrup, The permselectivity and water transference number of ion exchange membranes in reverse electrodialysis, J. Membr. Sci. 523 (2017) 402–408.
[28] B.J. Kim, R.Y. Kwak, H.J.J. Kwon, V. Sang Pham, M. Kim, B. Al-Anzi, G. Lim, J.Y. Hana, Purification of high salinity brine by multi-stage ion concentration polarization desalination, Sci. Rep. 6 (2016) 31850.
[29] R. Brown, E. Madrid, R. Castaing, J.M. Stone, A.M. Squires, K.J. Edler, K. Takashina, F. Marken, Free-standing phytantriol Q(224) cubic-phase films: resistivity monitoring and switching, ChemElectroChem 4 (2017) 1172–1180.
[30] B.B. Owen, F.H. Sweeton, The conductance of hydrochloric acid in aqueous solutions from 5 to 65°, J. Am. Chem. Soc. 63 (1941) 2811–2817.
[31] V.G. Artemov, A.A. Volkov, N.N. Sysoev, A.A. Volkov, Conductivity of aqueous HCl, NaOH and NaCl solutions: is water just a substrate? EPL 109 (2015) 26002.
[32] J.E. Hall, Access resistance of a small circular pore, J. Gen. Physiol. 66 (1975) 531–532.
[33] J.Y. Feng, J. Liu, B.H. Wu, G.L. Wang, Impedance characteristics of amine modified single glass nanopores, Anal. Chem. 82 (2010) 4520–4528.
[34] E.O. Barnes, G.E.M. Lewis, S.E.C. Dale, F. Marken, R.G. Compton, Generator-collector double electrode systems: a review, Analyst 137 (2012) 1068–1081.
[35] S.E.C. Dale, F. Marken, Electrochemistry within nanogaps, in: R.G. Compton, J.D. Wadhawan (Eds.), Nanoelectrochemistry, Electrochemistry-A Specialist Periodical Report, vol. 12, 2014, pp. 132–154.